Functional Topography of the Right Inferior Parietal Lobule Structured by Anatomical Connectivity Profiles

Jiaojian Wang,[1]* **Jinfeng Zhang,**[1] **Menglin Rong,**[1] **Xuehu Wei,**[1]
Dingchen Zheng,[1] **Peter T. Fox,**[2] **Simon B. Eickhoff,**[3,4] **and Tianzi Jiang**[1,5,6,7]*

[1]*Key Laboratory for NeuroInformation of the Ministry of Education, School of Life Science and Technology, University of Electronic Science and Technology of China, Chengdu, 625014, China*
[2]*Research Imaging Institute, University of Texas Health Science Center, San Antonio, Texas*
[3]*Institute of Neuroscience and Medicine (INM-1), Research Centre Jülich, Jülich, Germany*
[4]*Institute of Clinical Neuroscience and Medical Psychology, Heinrich Heine University, Dusseldorf, Germany*
[5]*Brainnetome Center, Institute of Automation, Chinese Academy of Sciences, Beijing, 100190, China*
[6]*National Laboratory of Pattern Recognition, Institute of Automation, Chinese Academy of Sciences, Beijing, 100190, China*
[7]*The Queensland Brain Institute, University of Queensland, Brisbane, Queensland, 4072, Australia*

◆ ━━ ◆

Abstract: The nature of the relationship between structure and function is a fundamental question in neuroscience, especially at the macroscopic neuroimaging level. Although mounting studies have revealed that functional connectivity reflects structural connectivity, whether similar structural and functional connectivity patterns can reveal corresponding similarities in the structural and functional topography remains an open problem. In our current study, we used the right inferior parietal lobule (RIPL), which has been demonstrated to have similar anatomical and functional connectivity patterns at the subregional level, to directly test the hypothesis that similar structural and functional connectivity patterns can inform the corresponding topography of this area. In addition, since the association between the RIPL regions and particular functions and networks is still largely unknown, post-hoc functional characterizations and connectivity analyses were performed to identify the main functions and cortical networks in which each subregion participated. Anatomical and functional connectivity-based parcellations of the RIPL have consistently identified five subregions. Our functional characterization using meta-analysis-based behavioral and connectivity analyses revealed that the two anterior subregions (Cl1 and Cl2) primarily participate in interoception and execution, respectively; whereas

the posterior subregion (Cl3) in the SMG primarily participates in attention and action inhibition. The two posterior subregions (Cl4, Cl5) in the AG were primarily involved in social cognition and spatial cognition, respectively. These results indicated that similar anatomical and functional connectivity patterns of the RIPL are reflected in corresponding structural and functional topographies. The identified cortical connectivity and functional characterization of each subregion may facilitate RIPL-related clinical research. *Hum Brain Mapp 00:000–000, 2016.*   © 2016 **Wiley Periodicals, Inc.**

Key words: right inferior parietal lobule; parcellation; structural connectivity; functional connectivity

---

INTRODUCTION

Fundamental to understanding the mechanisms of information processing in the human brain is relating structural connections to functional activity. Many previous studies have revealed that functional connectivity can reflect structural connectivity. Using empirical quantitative analyses of interregional structural and functional connectivity couplings, a number of previous studies revealed that dense structural connectivity (SC) tends to be strongly connected functionally [Hagmann et al., 2008; Honey et al., 2009; Koch et al., 2002; Skudlarski et al., 2008]. In addition, studies using functionally guided white matter pathway tractography demonstrated that functionally connected brain areas also showed direct structural connections [Greicius et al., 2009; Van den Heuvel et al., 2009]. Using computational modeling, a number of studies suggested that ongoing brain spontaneous fluctuations are highly structured [Deco et al., 2013, 2014; Honey et al., 2009].

The right inferior parietal lobule (RIPL) is one of the most important areas of the ventral attention network, which is largely lateralized to the right hemisphere [Corbetta and Shulman, 2002]. Compared with the left IPL, the RIPL is more involved in visuospatial attention processing, especially in attention reorientation [Fan et al., 2005]. Recently, using an anatomical connectivity-based parcellation approach, Mars et al. [2011] demonstrated that subregions of the right parietal cortex including the superior parietal lobule (SPL) and IPL showed similar anatomical and functional connectivity patterns. Subsequently, Wang et al. [2015b] utilized a connectivity-based parcellation approach to reveal convergent structural and functional architecture of the SPL. Thus, we hypothesized that similar structural and functional connectivity patterns of the RIPL can inform the corresponding topographical architecture of this area.

A connectivity-based parcellation approach is currently the best way to test whether the RIPL has corresponding structural and functional topographies. Recently, connectivity-based parcellation has been widely used to define functional subregions of the brain. On the basis of differences in their structural connectivity patterns, many cortical and subcortical areas have been parcellated to define their functional subregions [Anwander et al., 2007; Behrens et al., 2003; Fan et al., 2013; Johansen-Berg et al., 2004; Li et al., 2013; Liu et al., 2013; Mars et al., 2011; Neubert et al., 2014;

Sallet et al., 2013; Wang et al., 2012, 2015a, b; Zhang et al., 2014]. In addition to structural connectivity-based parcellation, resting-state functional connectivity [Cohen et al., 2008; Craddock et al., 2012; Kelly et al., 2012; Kim et al., 2010; Nebel et al., 2014; Wang et al., 2015b] has been used to identify subregions of brain. Using different types of connectivity patterns and then comparing the results could yield structural and functional topographies of brain areas and provide a new way to explore the relationship between structure and function.

Several previous studies have parcellated the RIPL using different modalities. Caspers et al. [2006] parcellated the IPL into seven subregions in both the left and right IPLs based on their regional cytoarchitectonic properties. Subsequently, Caspers and her colleagues demonstrated that the seven cytoarchitectonic subregions can be grouped into three clusters which have different receptor distribution patterns [Caspers et al., 2013]. Using an anatomical connectivity-based parcellation, Mars et al. [2011] subdivided the right parietal cortex into component subregions and identified five subregions in the RIPL, a parcellation scheme which was further supported by Wang and his colleagues' study [Wang et al., 2012]. Recently, Ruschel et al. parcellated the IPL into three subregions based on different anatomical connectivity patterns [Ruschel et al., 2014]. Although these previous studies proposed fine-grained subdivisions of the RIPL, the association between these RIPL subregions and specific functions and networks remains an open question.

The goal of this study was to test the hypothesis that similar structural and functional connectivity patterns can inform the corresponding topography using connectivity-based parcellation approaches. In addition, because of the lack of a detailed functional network investigation of the RIPL, we mapped the network that each subregion participated in using multimodal connectivity analyses. We also characterized the detailed functions that each subregion was involved in using a meta-analysis of behavioral domains and paradigms based on the BrainMap database.

MATERIALS AND METHODS

Definition of the Regions of Interest

The RIPL was defined on the basis of probabilistic cytoarchitectonic maps [Caspers et al., 2008], and a

maximum probability map (MPM) was calculated using the SPM Anatomy Toolbox [Eickhoff et al., 2005] (Fig. 1A). A definition of the RIPL that is based on a probabilistic cytoarchitectonic map can retain quantitative inter-subject variability information. Next, the RIPL seed mask in MNI space was transformed into each participant's individual diffusion space for fiber tracking and was resampled into 3 mm cubic voxels for the resting-state functional connectivity analyses.

Subjects

Ninety-six healthy, right-handed, undergraduate students subjects (55 males and 41 females, mean age = 20.5 years, standard deviation = 0.58) were recruited via advertisement. None of the participants had ever suffered from any psychiatric or neurological disease, and none had any contraindications for MRI scanning. All the subjects signed an informed consent before the MRI scanning. The study was in accordance with the latest revision of the declaration of Helsinki and had full ethical approval by the local Research Ethics Committee of the University of Electronic Science and Technology of China.

MRI Data Acquisition

All the subjects were scanned using a 3.0 Tesla GE MR Scanner. The DWI data included 64 images with non-collinear diffusion gradients ($b = 1000$ s/mm^2) and 3 non-diffusion-weighted images ($b = 0$ s/mm^2). A diffusion MRI for each participant was scanned using the following parameters: 75 slices, acquisition matrix = 128 × 128, flip angle (FA) = 90°, voxel resolution: 2 × 2 × 2 mm^3, and no gap. Sagittal 3D T1-weighted images were also acquired (TR/TE = 8.16/3.18 ms; inversion time = 800 ms; FA = 7°; FOV = 256 mm × 256 mm; matrix = 256 × 256; slice thickness = 1 mm, no gap; 188 sagittal slices). During the resting-state fMRI scanning, subjects were instructed to close their eyes and lie still and cushions were used to reduce head motion. Two hundred and fifty-five volumes of echo planar images were acquired (repetition time = 2,000 ms, echo time = 30 ms; no gap; 40 axial slices, voxel size, 3.75 × 3.75 × 4 mm^3).

Diffusion MRI Data Preprocessing

The data were preprocessed using the FSL software (http://www.fmrib.ox.ac.uk/fsl). Eddy currents and head motions were corrected. Skull-stripped T1-weighted images for each subject were co-registered to the subject's non-diffusion-weighted image ($b = 0$ s/mm^2) using a statistical parametric mapping (SPM8) package (http://www.fil.ion.ucl.ac.uk/spm). Next, the obtained T1 images (rT1) in diffusion space were transformed to the Montreal Neurological Institute (MNI) structural template. Finally, an inverse transformation was performed to transform the seed masks of the RIPL into the diffusion space for each subject for fiber tracking.

Resting-State fMRI Data Preprocessing

Preprocessing of the resting-state fMRI data was carried out using scripts provided by the 1,000 Functional Connectomes Project (www.nitrc.org/projects/fcon_1000) utilizing both the FSL and AFNI (http://afni.nimh.nih.gov/afni) softwares. To allow for magnetization equilibrium, the first 10 volumes were discarded. The slice timing for the remaining images was corrected, and the images were realigned to the first volume for head motion correction. The data from all the subjects with a maximum displacement of less than 1.5 mm and an angular motion of less than 1.5° were used in this study. On the basis of these criteria, 20 subjects were eventually discarded, and the data for the remaining 76 subjects were used for the subsequent analyses. All of the fMRI images were further normalized to the Montreal Neurological Institute (MNI) space using a structural MRI-based registration and were resampled to a 3 mm cubic voxel. Then, all the functional images were smoothed using a Gaussian kernel of 6 mm full-width at half maximum (FWHM). Finally, six motion parameters and the white matter, cerebrospinal fluid, and global mean signals were regressed out and filtered with a temporal band-path of 0.01–0.1 Hz.

First Set of Analyses: Connectivity-Based Parcellation of the RIPL

Anatomical connectivity-based parcellation of the RIPL

Diffusion probabilistic tractography was performed using the FSL package. Probability distributions were estimated for two fiber directions at each voxel [Behrens et al., 2007]. Probabilistic tractography was applied by sampling 5,000 streamline fibers in each voxel in the seed region to estimate the connectivity probability. To facilitate data storage and analysis, all of the connectivity patterns for each voxel were down-sampled to 5 mm isotropic voxels. The connectivity matrix consisted of rows indicating each RIPL voxel and columns representing each voxel of the whole brain (Fig. 1B). From this connectivity matrix, a symmetric cross-correlation matrix was generated (Fig. 1C). The size of this cross-correlation matrix was the number of voxels in the RIPL seed mask × the number of voxels in the RIPL seed mask of the RIPL, and the (i, j)th element value is the correlation between the connectivity profile of the RIPL voxel i and the connectivity profile of the RIPL voxel j [Johansen-Berg et al., 2004].

The similarity matrix was then grouped using spectral clustering for automated clustering to define different numbers of clusters from 2 to 9 [Fan et al., 2014; Wang et al., 2012, 2015a, b]. Then, the maximum probability map
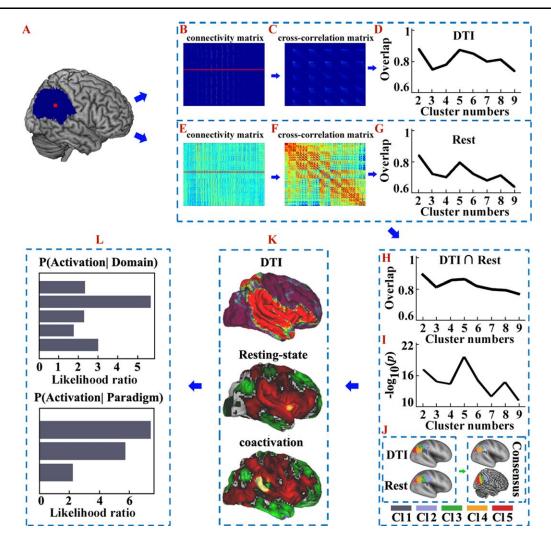
Figure 1.

Overall flowchart of this study. A. The right inferior parietal lobule (RIPL) mask was defined by probabilistic cytoarchitectonic maps using SPM Anatomy toolbox. B. Probabilistic tractography was performed from each voxel in the seed area and yielded a connectivity matrix between all voxels in the seed mask and each brain voxel. C. These anatomical connectivity matrices were then used to generate a symmetric cross-correlation matrix, which was then segmented for automated clustering to define different clusters/subregions. D. The overlap degree was calculated across all the subjects' parcellations at each cluster solution. E. The resting-state functional connectivity (RSFC) between each voxel in the seed area and each brain voxel was calculated to obtain a functional connectivity matrix. F. These RSFC matrices were then used to calculate a symmetric cross-correlation matrix using eta2. G. The overlap degree across all the subjects' parcellations at each cluster solution was computed to obtain the optimal number of clusters. H. The overlap degree between the maximum probability maps (MPM) yielded by anatomical and RSFC based parcellations was calculated and used to provide a complementary reference for determining the number of clusters. I. Statistical tests were used to detect significant overlap between the structural and functional connectivity-based parcellations of the RIPL. The negative logarithm of the statistical P-values was calculated and the biggest negative logarithm of the P-values was considered to be the optimal overlap across all the subjects. J. Anatomical and RSFC patterns-based parcellation approached were used separately to define the subregions. In this way the optimal five-way parcellation of the RIPL and the MPM for each subregion were calculated. The overlap of the MPMs yielded by the anatomical and RSFC-based parcellations was obtained and used to guide the subsequent analyses. K. The anatomical, RSFC, and task-related coactivation patterns for each RIPL subregion were mapped to identify the cortical network in which each subregion participated. L. A functional characterization, obtained using a meta-analysis of data from the BrainMap database, was used to determine the main functions for each RIPL subregion. [Color figure can be viewed in the online issue, which is available at wileyonlinelibrary. com.]

was created for each solution across all the subjects. To calculate the maximum probability map, we transformed each individual parcellation result from the diffusion space to the MNI152 template in MNI space. The maximum probability map, which used all the subjects' parcellation results in MNI space, was calculated by assigning each voxel of the reference space to the area in which it was most likely to be located. If two areas showed the same probability at a particular voxel, this voxel was assigned to the area with the higher average probabilities of the 26 voxels directly adjacent [Eickhoff et al., 2005; Wang et al., 2012].

Functional connectivity-based parcellation

To explore whether the RIPL has similarities between its structural and its functional topographies, we utilized resting-state functional connectivity patterns to subdivide the RIPL into different subregions. First, the RIPL seed masks were resampled into 3 mm cubic voxels, and the functional connections, computed using Pearson correlation coefficients between each voxel in the seed area and the other voxels in the rest of the brain, were calculated for each subject. Then, these functional connectivity maps were converted to z-score maps using the Fisher z transform (Fig. 1E). The similarity between the functional connectivity maps for every pair of voxels within the RIPL was computed using eta^2 [Cohen et al., 2008; Kelly et al., 2012; Nebel et al., 2012; Wang et al., 2015b]. This resulted in a correlation matrix in which the elements were the fraction of the variance in one functional connectivity map that was accounted for by the variance in a second functional connectivity map (Fig. 1F). The cross-correlation matrix was permutated using a spectral clustering method to parcellate the RIPL into 2–9 subregions [Fan et al., 2014; Wang et al., 2012, 2015a, b]. Next, the maximum probability map was created for each solution across all the subjects.

$$\text{eta}^2 = 1 - \frac{SS_{\text{within}}}{SS_{\text{combined}}} = 1 - \frac{\sum_{i=1}^{n}(a_i - m_i)^2 + (b_i - m_i)^2}{\sum_{i=1}^{n}(a_i - \bar{M})^2 + (b_i - \bar{M})^2}$$

where, a_i and b_i are the values at position i in the functional connectivity maps a and b, respectively, m_i is the mean value of the two functional connectivity maps at position i, and $\bar{M}$ is the grand mean across all locations in both correlation maps.

Determining the number of clusters

In this study, we used the generalized Dice coefficient as an index to determine the final number of clusters [Dice, 1945; Wang et al., 2015b]. The maximum consistency across all the subjects' parcellation results obtained from the anatomical or resting-state functional connectivity patterns was set as the optimal number of clusters. In

addition, we calculated the overlap degree between the maximum probability maps yielded by an anatomical or resting-state functional connectivity-based parcellation to provide the results of a complementary method as a reference for determining the number of clusters.

$$\text{Dice coefficient} = \frac{A \cap B}{A \cup B}$$

In addition, we used a statistical analysis to determine the amount of significant overlap between the structural and functional connectivity-based parcellations of the RIPL. The main procedures were as follows: First, we registered the structural connectivity-based parcellation results for the RIPL in diffusion space to the standard MNI space. Then, we re-sampled the structural connectivity and functional connectivity-based parcellation results into 1 mm cubic voxels. Next, we calculated the degree of overlap between the structural and functional connectivity-based parcellations of the RIPL in each subject. Subsequently, a one-sample t-test was used to determine the significance and a P-value was obtained. Finally, the negative logarithm of the P-values was calculated to detect the significance, and the biggest negative logarithm of the P-value was considered to be the optimal overlap across all the subjects. The optimal solution for RIPL was used to guide the further analyses.

Second Set of Analyses: Connectivity and Functional Characterization of the RIPL Subregions

Whole brain structural connectivity patterns

To investigate the relationship between structure and function, we mapped the whole brain structural, resting-state functional, and task-related coactivation patterns for each of the derived clusters (Fig. 1K). To map the whole brain anatomical connectivity pattern of each subregion of the RIPL, we transformed the seed masks to diffusion space and used Probtracking [Behrens et al., 2003] to obtain the connectivity probability between each subregion of the RIPL and all the other voxels in the brain. We drew 5,000 samples from the connectivity distribution for each voxel and calculated the connection probability for each voxel. Finally, we transformed the identified fiber tracts into MNI space and averaged all the connection probability maps to obtain a mean probability connectivity map for each subregion.

Whole brain resting-state functional connectivity

To determine the whole brain resting-state functional connectivity (RSFC) patterns for each subregion, we first resampled the subregions to 3 mm cubic voxels in MNI space. In the current study, the FC was defined by the correlations between the time series. The Pearson correlation

coefficients between the mean time series for each seed region and the mean time series for each voxel of the whole brain were calculated for each subject and then converted to z values using Fisher's z transformation to improve normality. Then each individual's z-values were entered into a random effects one-sample t-test in a voxel-wise manner to determine the regions that showed significant correlations with the seed region. Finally, the functional connectivity map was thresholded at a cluster-level FWE-corrected threshold of $P < 0.05$ (cluster-forming threshold at voxel-level $P < 0.001$)

Whole brain coactivation connectivity

The task-dependent co-activated functional connectivity of each subregion was mapped using a structure-based meta-analysis and meta-analytic connectivity modeling (MACM) approach [Eickhoff et al., 2010; Laird et al., 2013; Robinson et al., 2010]. The data was obtained from the BrainMap database and included the data that had at least one focus of activation in a particular connectivity-based parcellation-yielded subregion. Structure-based meta-analyses are based on the co-occurrence of spatially separate neurophysiological events. The main procedures of the MACM analyses were as follows. First, we retrieved for each of the subregions yielded by a tractography-based parcellation all of the studies from the BrainMap database that reported activation within that particular subregion. Note that we considered all eligible BrainMap experiments because any pre-selection based on taxonomic categories would have constituted a strong a priori hypothesis about how brain networks are organized. However, how well psychological constructs, such as emotion and cognition, map regional brain responses is unclear. In other words, the experiments we used were defined purely based on location not by the type of experiment or the contrast they probed in yielding unbiased maps of whole-brain co-activations. In turn, the subsequent functional characterization then probed the types of the paradigm classes and behavioral domains that were featured by the experiments that activated each subregion. Then, an activation likelihood estimation (ALE) meta-analysis was performed on the obtained experiments, and statistical inference calculations were done to establish which brain regions were significantly coactivated with a particular subregion of the RIPL. The key idea behind ALE is to treat the foci reported in the associated experiments not as single points but as centers for 3D Gaussian probability distributions that reflect the spatial uncertainty associated with neuroimaging results. For each experiment, the probability distributions for all the reported foci were then combined into a modeled activation (MA) map for that particular experiment. The voxel-wise union of these MA (modeled activation)-values for all the experiments associated with a particular seed voxel then yielded an ALE score for each voxel of the brain that describes the co-activation probability of that particular location with the current seed voxel. No

threshold was applied to retain the complete pattern of co-activation likelihood [Eickhoff et al., 2009]. The ALE score for the MACM analysis of each cluster was compared with a null-distribution that reflected a random spatial association between experiments with a fixed within-experiment distribution of foci [Eickhoff et al., 2009]. This random-effects inference assesses the above-chance convergence between experiments rather than the clustering of foci within a particular experiment. The observed ALE scores from the actual meta-analysis of the experiments activated within a particular subregion were then tested against the ALE scores obtained under this null-distribution, yielding a P-value based on the proportion of the equal or higher random values [Eickhoff et al., 2012]. These non-parametric P-values were converted to z-scores and thresholded at $P < 0.05$ (cluster-level FWE-corrected, cluster-forming threshold at voxel-level $P < 0.001$).

Overlap and specific networks

We mapped the overlap networks formed by overlapping the RSFC and coactivation networks. To calculate the overlap network shared by the whole brain RSFC patterns and the coactivation patterns for each subregion, we initially computed whole brain RSFC and task-related coactivation networks for each RIPL subregion, as described above. Next, both the coactivation and the RSFC maps were thresholded at a FWE-corrected cluster-level threshold of $P < 0.05$ (cluster-forming threshold at a voxel-level $P < 0.001$). Finally, a conjunction analysis (i.e., the intersection connectivity analysis) was performed to calculate the overlap between the two networks for each subregion.

In addition, we mapped the specific overlap networks for each subregion to reveal the unique RSFC and task-dependent coactivation patterns. The specific networks were the brain areas that were significantly more coupled with a given subregion than with any of the others.

Functional characterization: behavioral domain analysis

The functional characterization of the connectivity-based parcellation-yielded subregions was used to identify the main functions for each subregion based on analyses of the behavioral domains and paradigm classes in the Brain-Map database (Fig. 1L). The behavioral domain analysis results included five behavioral domains (Action, Cognition, Emotion, Interoception, and Perception) and 51 behavioral sub-domains. Paradigm class analyses primarily categorize the specific task employed. A functional characterization of each subregion yielded by the connectivity-based parcellation was determined using forward inferences [Bzdok et al., 2013; Cieslik et al., 2013; Clos et al., 2013; Rottschy et al., 2013]. Forward inference represents the probability of observing activity in a brain region given knowledge about psychological processes. Based on the forward inference approach, a subregion's

functional profile was determined by identifying the taxonomic labels (domains or subdomains) for which the probability of finding activation in a specific subregion was significantly higher than the overall chance (across the entire database) of finding activation in that particular subregion. The significance was established using a binomial test ($P < 0.05$ corrected for multiple comparisons using the false discovery rate [FDR] method) [Eickhoff et al., 2011].

RESULTS

First Set of Analyses: Connectivity-Based Parcellation of the RIPL

Correspondence between the structural and functional topographies of the RIPL

In this study, we tested whether similar anatomical and functional connectivity patterns could reveal corresponding similarities in the structural and functional topographies of the RIPL using a connectivity-based parcellation approach. The overall approach of the study is shown in Figure 1. The maximum consistency across all the subjects' parcellation results obtained from the anatomical or resting-state functional connectivity patterns identified the optimal five subregions of RIPL (Fig. 1D,G). In addition, the overlap degree between the maximum probability maps yielded by an anatomical or resting-state functional connectivity-based parcellation also identified the optimal five-way parcellation of RIPL (Fig. 1H), and the subsequent statistical test for the overlap across all the subjects also revealed that the five-way parcellation of the RIPL was the optimal one ($P_{k=2} = 2.0883 \times 10^{-18}$, $P_{k=3} < 9.3180 \times 10^{-14}$, $P_{k=4} < 2.0487 \times 10^{-15}$, $P_{k=5} < 3.2635 \times 10^{-22}$, $P_{k=6} < 6.9076 \times 10^{-16}$, $P_{k=7} < 7.4746 \times 10^{-12}$, $P_{k=8} < 5.1004 \times 10^{-14}$, $P_{k=9} < 3.6401 \times 10^{-13}$) (Fig. 1I). These analyses revealed a five-way parcellation of the RIPL as the optimal solution, which was used to guide the further analyses (Fig. 1J). The anatomical and functional topographies of the RIPL were found to be consistent with the cytoarchitectonic maps of this area by calculating the overlap degree between each RIPL subregion yielded by the connectivity-based parcellation and each cytoarchitectonic subregion (Fig. 2). The consensus of the RIPL parcellation results was: The most anterior clusters were Cluster 1 (gray/Cl1) and Cluster 2 (light blue/Cl2), which were posterior to the postcentral sulcus. Cluster 1 was ventral to Cluster 2 and corresponded to the cytoarchitectonically defined area PFcm [Caspers et al., 2008] (Fig. 2), whereas the dorsal Cluster 2 was similar in location to the cytoarchitectonically defined area PFt [Caspers et al., 2008] (Fig. 2). Cluster 3 (dark green/Cl3) was posterior to Cluster 2 and resembled area PFm [Caspers et al., 2008], as defined by cytoarchitecture (Fig. 2). Cluster 4 (green/Cl4) was located on the anterior AG and was similar in location to the cytoarchitectonically defined area PGa [Caspers et al., 2008] (Fig. 2). The most posterior cluster in the RIPL was Cluster 5 (red/Cl5), which resembled
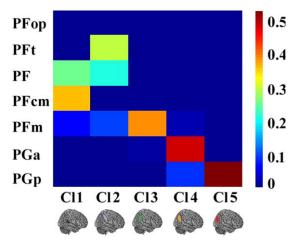

Figure 2.
Overlap between the RIPL subregions defined using a connectivity-based parcellation and cytoarchitecture. The quantitative overlap between the overlap of each subregion yielded by anatomical connectivity and the RSFC-based parcellation and each cytoarchitectonic subregion of RIPL was computed. [Color figure can be viewed in the online issue, which is available at wileyonlinelibrary.com.]

cytoarchitectonic subdivision PGp [Caspers et al., 2008] (Fig. 2). Furthermore, the consensus structural and functional topographies of the RIPL were also consistent with a previous anatomical connectivity patterns-based parcellation of the right parietal cortex, which also identified five RIPL subregions arranged rostrally to caudally [Mars et al., 2011].

Second Set of Analyses: Connectivity and Functional Characterization of the RIPL Subregions

Whole brain anatomical connectivity

The whole brain structural connectivity patterns of each subregion of the RIPL were mapped using probabilistic tracking (Fig. 3B). In addition, we randomly selected five subjects' tracking results in individual diffusion space and displayed them on the individual diffusion images (Supporting Information Fig. S1). For the first subregion (Cl1), the primary anatomical connections were found in the bilateral parietal opercula, superior and middle temporal gyri, inferior frontal gyrus, insula, caudate, superior parietal lobule, and thalamus via the corpus callosum (CC), corticospinal tract (CST), superior longitudinal fasciculus (SLF) III, and extreme capsule (EmC) [Makris et al., 2005; Makris and Pandya, 2009]. The structural connectivity patterns of Cl2 were found to primarily connect to the superior parietal lobule, postcentral gyrus, inferior frontal gyrus, insula, ventral and dorsal premotor cortex, superior temporal gyrus, posterior middle temporal gyrus, inferior temporal gyrus, caudate, and thalamus through the SLFII,
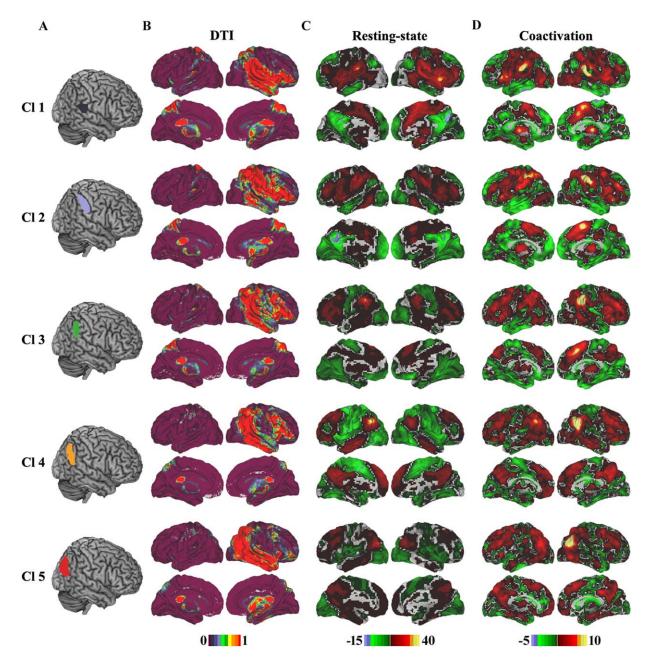
Figure 3.

Whole brain anatomical, resting-state functional, and coactivation connectivity patterns for each subregion of the right inferior parietal lobule (RIPL). A. Each subregion of the RIPL was overlaid on the structural template. B. Whole brain population maps of the probabilistic tractography results of each subregion of the RIPL. The main tract pathways include the superior longitudinal fasciculus (SLF), extreme capsule (EmC), corticospinal tract (CST), and corpus callosum (CC). C. Whole brain resting-state functional connectivity patterns for each cluster were obtained using one sample t-tests (thresholded at $P < 0.05$, cluster-level FWE-corrected, cluster-forming threshold at voxel-level $P < 0.001$). D. The whole brain coactivation connectivity pattern for each subregion of the RIPL was obtained using meta-analytical connectivity modeling (MACM) analyses (thresholded at $P < 0.05$, cluster-level FWE-corrected, cluster-forming threshold at voxel-level $P < 0.001$). [Color figure can be viewed in the online issue, which is available at wileyonlinelibrary.com.]

SLFIII, EmC, inferior longitudinal fascicules (ILF), CC, and CST. Cl3 primarily connected with the inferior frontal gyrus, insula, superior parietal lobule, postcentral gyrus, ventral and dorsal premotor cortices, middle frontal gyrus, posterior middle temporal gyrus, inferior temporal gyrus, caudate, and thalamus. The connectivity patterns of Cl4 were mainly with the inferior and middle frontal gyri, anterior insula, posterior middle temporal gyrus, inferior temporal gyrus, caudate, and thalamus via the ILF, SLFII, SLFIII, and CST. The most posterior subregion, Cl5, predominantly connected with the superior, middle, and inferior temporal gyri, superior and middle frontal gyri, insula, caudate, and thalamus via the ILF, SLFI, SLFII and CST.

Whole brain resting-state functional connectivity

The whole brain resting-state functional connectivity of each subregion identified by connectivity-based parcellation was mapped to reveal its intrinsic functional organization (Fig. 3C). The resting-state functional connectivity patterns of the RIPL subregions were very similar to those of the structural connectivity patterns. For Cl1, the primary functional connections were found to be with the bilateral inferior frontal gyrus, anterior middle frontal gyrus, insula, precentral and postcentral gyri, superior temporal gyrus, posterior middle temporal gyrus, supplementary motor area, anterior cingulate cortex, caudate, and thalamus. Cl2 was primarily correlated with the bilateral inferior and middle frontal gyri, postcentral and precentral gyri, posterior middle and inferior temporal gyri, supplementary motor area, anterior cingulate cortex, caudate, and thalamus. Cl3 was primarily functionally connected with the superior, middle, and inferior frontal gyri, medial anterior frontal cortex, anterior and posterior cingulate cortex, and thalamus. The functionally correlated brain areas for Cl4 were in default mode network-related areas including the dorsolateral prefrontal cortex, anterior temporal gyrus, precuneus, and medial prefrontal cortex. Cl5 mainly connected with the superior and middle frontal gyri, frontal pole, inferior temporal gyrus, medial frontal cortex, precuneus, thalamus, and parahippocampus.

Whole brain coactivation connectivity

The whole brain coactivation connectivity pattern for each subregion was obtained using meta-analysis connectivity modeling (MACM). The coactivation connectivity pattern for each subregion was very similar with each resting-state functional connectivity pattern (Fig. 3D). For Cl1, compared with the RSFC patterns, coactivation connectivity was additionally found in the visual cortex. For Cl2, coactivation connectivity was additionally observed in the visual cortex, whereas RSFC was additionally found in the posterior inferior temporal gyrus. Cl3 additionally coactivated with the anterior visual cortex, whereas the RSFC of Cl3 was additionally observed in the middle

cingulate cortex. Coactivated brain areas for Cl4 were additionally found in the visual cortex, inferior and middle frontal gyri, and ventral postcentral gyrus. The extra coactivation brain areas for Cl5 were primarily observed in the anterior occipital gyrus, supplementary motor area, and anterior middle temporal gyrus, whereas additional RSFC was found in the inferior temporal gyrus.

Overlap and specific network

We mapped the intersection of the resting-state functional and coactivation connectivity patterns to characterize the correspondence between the resting-state and task-related coactivation networks. This intersection was mapped by determining the connectivity shared by both types of networks (Fig. 4B). The conjunct connectivity of subregion 1 (Cl1) was found in the bilateral inferior frontal gyri and insula, right posterior middle temporal gyrus, bilateral supplementary motor area, and right middle cingulate cortex. For Cl2, conjunct connectivity was primarily observed in the bilateral insula, inferior frontal gyrus, posterior inferior frontal sulcus, anterior middle frontal gyrus, superior frontal gyrus, and pre-supplementary motor area. The conjunctions between the two types of connectivity for Cl3 were found in the bilateral middle and inferior frontal gyri, insula, and right pre-supplementary motor area. The overlap between the functional and coactivation connectivity of Cl4 was primarily found in the bilateral middle frontal gyri, pre-supplementary motor area, posterior cingulate gyrus, and right middle temporal gyrus. Conjunct functional and coactivation connectivity for Cl5 was predominantly observed in the left superior and middle frontal gyri and bilateral precuneus.

In addition, we mapped the specific RSFC and coactivation patterns of each RIPL subregion to identify the unique connectivity patterns for each subregion (Fig. 5B). The connections that were specific for Cl1 were found in the bilateral inferior frontal gyri, supplementary motor area, and superior temporal gyrus. Cl2 was specifically connected with the bilateral dorsal premotor cortex. The specific RSFC and coactivation areas for Cl3 were found in the left inferior parietal lobule and right inferior frontal sulcus. Cl4 had specific connections with the precuneus and posterior middle temporal gyrus. Cl5 was specifically connected with the left inferior parietal lobule and frontal eye field.

Functional characterization: behavioral domain and paradigm analysis

We used quantitative forward inferences on the behavioral domains and paradigm classes to determine the functional organization of each RIPL subregion. The significant activation probabilities within a subregion given a certain taxonomic label (forward inference) were recorded (Fig. 6). Functional characterization revealed that the ventral anterior subregion (Cl1) primarily participated in
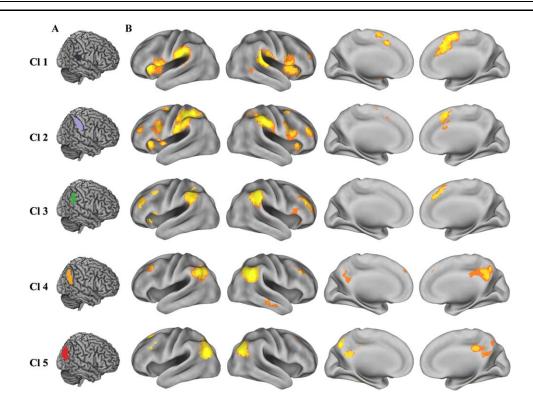
Figure 4.

Overlapping connectivity between the resting-state functional and coactivation connectivities. A. Each subregion of the RIPL was overlaid on the structural template. B. The intersection connectivity was calculated using the whole brain resting-state functional and coactivation connectivities. We first obtained thresholded (thresholded at P < 0.05, cluster-level FWE-corrected, cluster-forming threshold at voxel-level P < 0.001) whole brain resting-state functional connectivity and coactivation connectivity maps of each right inferior parietal lobule (RIPL) subregion and then computed the intersection connectivity between the two modalities. [Color figure can be viewed in the online issue, which is available at wileyonlinelibrary.com.]

interoception, emotion, somesthesis, execution, and auditory perception. The dorsal anterior subregion (Cl2) was mainly involved in somesthesis, execution, and tactile processing. The subregion of Cl3 mainly participated in inhibition and attention related processing. The anterior subregion in the AG was Cl4, and its main functions included social cognition and reasoning. The posterior subregion in the AG was Cl5, which primarily participated in spatial cognition and imagined objects or scenes.

DISCUSSION

In our current study, we demonstrated that similar anatomical and functional connectivity patterns can reveal a corresponding topographic architecture of the RIPL. Previous studies have revealed correspondence between large-scale networks defined by resting-state functional connectivity and brain structural connectivity [Greicius et al., 2009; Van den Heuvel et al., 2009]. This correspondence was also reflected in the consistent functional and structural topography of the RIPL. In addition, together with evidence

of a strong correspondence between the anatomical and functional networks, our findings supported the hypothesis that the fundamental topographical organization of the brain can be revealed by comparing the results obtained using different connectivity patterns. This means that the fundamental brain architecture can be detected in multiple neuroimaging techniques and that the large-scale connectivity patterns detected by different methods and modalities share a common basis [Kelly et al., 2012; Wang et al., 2015b].

The observed whole brain structural connectivity, resting-state functional connectivity, and coactivation patterns for the RIPL subregions were quite similar across different modalities. The similar connectivity pattern between the anatomical and functional connectivity indicated that the functional networks of the RIPL subregions are implemented by the anatomical connectivity and that neuronal activity reflects direct physical connectivity [Deco et al., 2013; Zhang et al., 2010]. However, some divergence between different types of connectivity patterns was also observed. The observed divergence between the task-independent rest-state and the task-dependent coactivation connectivity may relate to the fundamental differences between the two states. The coactivations
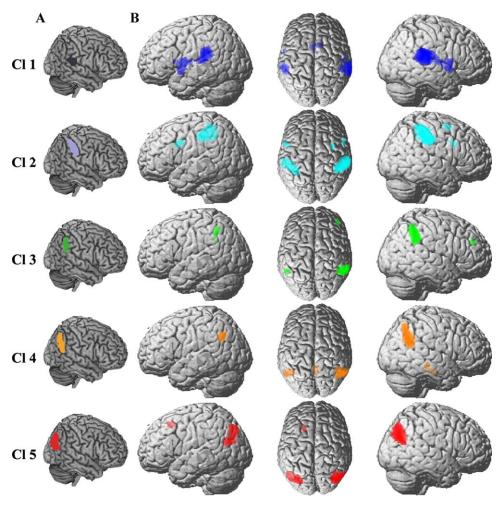
Figure 5.

The specific resting-state and coactivation connectivity pattern of each right inferior parietal lobule (RIPL) subregion. A. Each subregion of the RIPL was overlaid on the structural template. B. The brain areas significantly more correlated and coactivated with a given subregions than with any of the other subregions of RIPL. [Color figure can be viewed in the online issue, which is available at wileyonlinelibrary.com.]

primarily reflect patterns of coordinated activity in response to external task demands in a broad range of tasks, whereas the resting-state functional connectivity mainly reflects spontaneous networks related to self-initiated behavior and, thus, cannot be completely mirrored by coactivation networks [Eickhoff and Grefkes, 2011]. Compared with the amount of divergence between the resting-state functional connectivity and the coactivation patterns, greater differences were found between the anatomical and the functional connectivity patterns, especially in their contralateral hemispheric connections. This great discrepancy may have resulted from an intrinsic limitation of the diffusion MRI technique, which has difficulty tracing long-range connections, especially contralateral hemispheric connections.

Previous anatomical and functional connectivity analyses of the RIPL subregions revealed different connectivity properties [Caspers et al., 2011; Mars et al., 2011]. The anterior subregion that corresponded to the PFop cytoarchitectonic area primarily connected to the ventral premotor area (PMv), whereas the dorsal subregion that corresponded to PFt cytoarchitectonic area mainly connected with dorsolateral prefrontal cortex (dlPFC). The middle subregion, which is similar to the PF defined by cytoarchitecture, was primarily connected to the dlPFC and anterior prefrontal cortex (aPFC). The posterior two subregions in the AG, corresponding to cytoarchitectonic areas PGa and PGp, were primarily connected to the aPFC and parahippocampus (PH). The specific connections patterns for areas PFop and PF were consistent with our specific resting-state functional connectivity and coactivation patterns analyses for the two corresponding areas, Cl1 and Cl3. However, the specific connectivity patterns for the
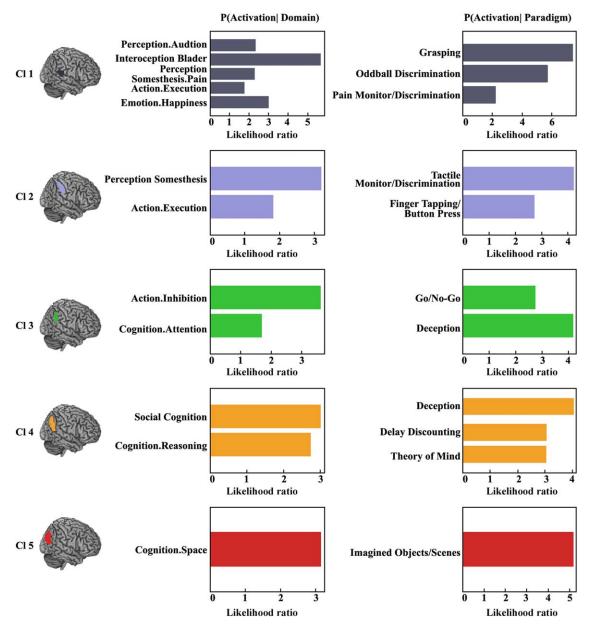
Figure 6.

Behavioral domains and paradigm classes for the right inferior parietal lobule (RIPL) subregions. Forward inference was used to determine the functional organization of each subregion. The significant activation probabilities for each subregion with respect to a given domain or paradigm in a cluster are depicted separately. [Color figure can be viewed in the online issue, which is available at wileyonlinelibrary.com.]

PFt, PGa, and PGp areas, which approximately corresponded to areas Cl2, Cl4, and Cl5, respectively, in our current study, were different. The specific functional connections for Cl2 were found in the dorsal and ventral premotor cortex. Cl4 and Cl5 were specifically connected to the posterior middle temporal gyrus and the frontal eye field, respectively. The differences in the functional connectivity patterns for areas Cl2, Cl4, and Cl5 (corresponding to

cytoarchitectonic areas PFt, PGa, and PGp, respectively) may have resulted from the different analytic methods. Mars et al. [2011] used a target-to-seed method to calculate the functional connectivity between each target area and each voxel of the whole parietal cortex to identify which parts of the parietal cortex significantly connected with the target area. Thus, the specifically connected brain areas of each RIPL subregion were limited. In contrast, we used a

seed-to-whole brain method to calculate the whole brain functional connectivity patterns of each RIPL subregion to identify the specific connectivities, which may clarify the specific connectivity patterns for the RIPL subregions throughout the whole brain. In addition, the specific connectivity that we obtained was the result of the intersection between the resting-state functional and the task-related coactivation connectivities for each RIPL subregion. This method, thus, may reduce the number of brain areas which might connect specifically with different RIPL subregions.

The most ventral-rostral Cl1 was found to abut the parietal operculum and temporoparietal junction area. The anatomical location of this cluster suggests that this area may be involved in many cognitive functions. The functional characterization of Cl1 indeed revealed that this area participated in different types of functions, including audition, action, somesthesis, and even emotion. Previous anatomical connectivity analyses indicated that the contralateral corresponding area plays an important role in transferring auditory input to motor output [Catani et al., 2005; Hickok and Poeppel, 2000]. Thus, Cl1 plays an important role in phonological processing and is part of the phonological network [Graves et al., 2010]. In addition, the functional characterization of Cl1 showed that this area is primarily involved in interoception. This finding suggests that Cl1 plays an important role in representations of bodily responses and subjective feeling states [Craig, 2002, 2003; Critchley et al., 2004]. The dorsal-anterior Cl2, which primarily corresponds to cytoarchitectonic area PFt, was reported to be involved primarily in action observation and imitation, suggesting that Cl2 may be part of the mirror neuron system [Caspers et al., 2010; Rizzolatti, 2005]. However, the behavioral analyses in our current study indicated that Cl2 participated in somesthesis and execution and, thus, may be mainly involved in directing visually guided action [Frey et al., 2005], a concept which was supported by its specific connectivity patterns with the ventral and dorsal premotor (PMd and PMv) cortex. In addition, the specific connectivity patterns of Cl2 with the PMd and PMv, considering the different functional roles of the PMd and PMv [Tomassini et al., 2007], hinted that this area may be further parcellated into component subregions. The middle subregion of Cl3, which mainly corresponds to the PFm defined by cytoarchitecture, was related to changes in response strategy [Boorman et al., 2009] and exploratory decisions [Daw et al., 2006] in previous fMRI based studies. Cl3 was also shown to be involved in reevaluating conflicting choice options as well as in spatial attention and reorienting tasks [Caspers et al., 2013; Mevorach et al., 2009; Vossel et al., 2006], which were consistent with the findings of the functional characterization using meta-analysis in our current study of this area. Taken together, Cl3 maybe primarily contribute to rule changes during visually guided attention [Corbetta and Shulman, 2002]. The most posterior two subregions are mainly located on the angular gyrus. The anterior angular subregion was Cl4, which has primarily been considered to participate in the inhibition of inappropriate responses across a variety of go/no-go tasks, unlike the left anterior subregion in the angular area, which has primarily been found to be involved in language processing [Nee et al., 2007; Wager et al., 2005]. However, the meta-analyses in our current study suggested that this area primarily participated in higher cognitive functions, including social cognition and reasoning. This discrepancy may result from our meta-based behavioral analysis approach, which identified the most significant functions associated with this area. However, finding these associations does not mean that this area is not involved in other functions. In addition, the functional characterization of this area in our current study was supported by its specific connectivity with the posterior middle temporal gyrus and precuneus and by the previous theory-of-mind or mentalizing tasks findings that were based on fMRI studies [Gallagher et al., 2000; Mar, 2011; Raine and Yang, 2006; Spreng et al., 2009]. These findings suggested that Cl4 may still be a functionally heterogeneous area which could be further parcellated using high resolution MRI. The most posterior subregion, Cl5, primarily participated in spatial cognition, according to our study. The functional characterization for this area is consistent with previous anatomical connectivity analyses of the corresponding cytoarchitectonic area, PGp, which primarily connected with extrastriatal visual areas for spatial processing [Caspers et al., 2011]. In addition, resting-state functional connectivity and anatomical connectivity analyses of this area revealed that it strongly connects with the parahippocampus and may contribute to spatial navigation [Uddin et al., 2010].

The structural and functional asymmetry of the IPL between the left and the right hemispheres has been documented in many previous studies [Caspers et al., 2006; Gorno-Tempini et al., 2004; Smith et al., 1987; Vesia et al., 2006]. The asymmetric anatomical connectivity patterns of the cytoarchitectonic left and right IPL subregions were also identified using a probabilistic fiber tracking approach [Caspers et al., 2011], which provided a neuroanatomical basis for the functional asymmetry. However, whether the asymmetric connectivity patterns result in different functional topographies for the left and the right IPL is controversial. In our current study, using a connectivity-based parcellation approach, we further demonstrated that asymmetric connectivity patterns can generate differences in the functional topographical architecture of the brain.

Visuospatial attention is controlled by the dorsal and ventral attention network, and the ventral attention network, primarily including the right inferior frontal gyrus and inferior parietal lobule, is largely lateralized to the right hemisphere [Corbetta and Shulman, 2002]. Previous task-based fMRI studies revealed that the angular gyrus is primarily involved in visuospatial attention processing, especially in attention reorientation [Fan et al., 2005; Mort et al., 2003]. More recently, Mars et al. [2012] used an

anatomical connectivity-based parcellation approach to parcellate the right temporoparietal junction (TPJ) including the IPL, and found that the anterior TPJ, not the IPL that we found, primarily participated in the attention network. The inconsistencies between their findings and ours may have been caused by differences in the analysis methods and/or by inexact anatomical localization. The task-based fMRI detected the functional activation and revealed the approximately anatomical location. Mars et al. [2012] used a parcellation approach to subdivide the TPJ and resting-state functional connectivity to evaluate the functional network in which each TPJ subregion participated. However, resting-state functional connectivity analyses only identify the network that is involved in the resting state although some studies reported corresponding networks at rest and during tasks [Smith et al., 2009; Wang et al., 2015a,b]. Whether resting-state networks can completely inform task-related networks, especially the task-dependent positive activation network, still needs to be validated. Thus, the inferential ability of resting-state network analyses to elucidate task-related networks also needs to be further confirmed. Furthermore, the ability to reorient attention was tested by comparing invalidly cued with validly cued trials identifying the brain areas related to inhibition control [Thiel et al., 2004]. Thus, the ability to inhibit information plays an important role in reorienting attention. In our current study, we used a structure-based meta-analysis of a number of previous task-related fMRI studies pooled in the BrainMap database to identify the main functions for each subregion. This method can better and more reliably identify the associated functions for a specific brain area. The behavioral domain and paradigm analyses of the IPL subregions revealed that Cl3 primarily participated in inhibition and attention and suggested that Cl3 in the RIPL plays a key role in attention reorientation. Our finding was supported by previous anatomical connectivity analyses, which revealed that the between-hemispheric asymmetry of the anatomical connections of the IPL with the middle and inferior frontal gyri underlies the lateralization of visuospatial attention [Thiebaut de Schotten et al., 2011; Wu et al., 2016].

There are also limitations to our current study. During the resting-state fMRI data preprocessing, we did not exclude the physiological signals, such as respiration and heart rate, because we did not collect these data during the fMRI scanning. Because these physiological signals can affect the blood-oxygen level dependent (BOLD) signal, the whole brain resting-state functional connectivity (RSFC) pattern may be affected [Chang et al., 2009]. In addition, during the preprocessing of the fMRI data, we regressed out the global mean signal to map the whole brain RSFC patterns. Many previous studies have shown that global mean regression can lead to spurious resting-state functional correlations and false inferences, particularly when comparing groups of participants [Gotts et al., 2013a,b; Saad et al., 2013]. However, regressing out the global mean signal can also identify stable brain networks, such as the default mode network [Andrews-Hanna et al., 2010; Power et al., 2011]. Thus, whether to regress out the global mean signal for the fMRI data during preprocessing remains controversial. To validate the RSFC patterns for each RIPL subregion and identify the stable functional connectivity patterns, we further mapped the task-related coactivation patterns and overlapped them with the whole brain RSFC patterns for each RIPL subregion. The overlap between the functional connectivity patterns at rest and under task indicated that the resting-state functional connectivity pattern for each subregion is reliable.

In summary, we demonstrated that corresponding topographical architecture of the RIPL can be revealed on the basis of similar anatomical and functional connectivity patterns. The maximum consistent parcellation of the RIPL across different modalities identified five subregions, and this parcellation result was similar to cytoarchitectonical maps and previous anatomical connectivity-based parcellations. The three anterior subregions in the SMG (Cl1, Cl2, and Cl3) resemble the areas PFop, PFt, and PFm defined by cytoarchitecture, respectively. The two posterior subregions resemble the cytoarchitectonic areas PGa and PGp, respectively. Functional characterization of each RIPL subregion revealed that the three anterior subregions Cl1, Cl2, and Cl3 in the SMG primarily participated in execution, somesthesis processing, and action inhibition, respectively, whereas the two posterior subregions (Cl4, Cl5) in the AG were primarily involved in social cognition and spatial cognition, respectively. Furthermore, these functionally different subregions were supported by their distinct structural, resting-state functional, and coactivation connectivity patterns. The cortical connectivity patterns and functional characterization of each subregion may facilitate future RIPL-related clinical and cognitive neuroscience research.

REFERENCES

Andrews-Hanna JR, Reidler JS, Sepulcre J, Poulin R, Buckner RL (2010): Functional-anatomic fractionation of the brain's default network. Neuron 65:550–562.

Anwander A, Tittgemeyer M, von Cramon DY, Friederici AD, Knosche TR (2007): Connectivity-based parcellation of broca's area. Cereb Cortex 17:816–825.

Behrens TE, Johansen-Berg H, Woolrich MW, Smith SM, Wheeler-Kingshott CA, Boulby PA, Barker GJ, Sillery EL, Sheehan K, Ciccarelli O, Thompson AJ, Brady JM, Matthews PM (2003): Non-invasive mapping of connections between human thalamus and cortex using diffusion imaging. Nat Neurosci 6: 750–757.

Behrens TE, Berg HJ, Jbabdi S, Rushworth MF, Woolrich MW (2007): Probabilistic diffusion tractography with multiple fibre orientations: What can we gain? NeuroImage 34:144–155.

Boorman ED, Behrens TE, Woolrich MW, Rushworth MF (2009): How green is the grass on the other side? Frontopolar cortex and the evidence in favor of alternative courses of action. Neuron 62:733–743.

Bzdok D, Laird AR, Zilles K, Fox PT, Eickhoff SB (2013): An investigation of the structural, connectional, and functional subspecialization in the human amygdala. Hum Brain Mapp 34:3247–3266.

Caspers S, Geyer S, Schleicher A, Mohlberg H, Amunts K, Zilles K (2006): The human inferior parietal cortex: cytoarchitectonic parcellation and interindividual variability. NeuroImage 33:430–448.

Caspers S, Eickhoff SB, Geyer S, Scheperjans F, Mohlberg H, Zilles K, Amunts K (2008): The human inferior parietal lobule in stereotaxic space. Brain Struct Funct 212:481–495.

Caspers S, Zilles K, Laird AR, Eickhoff SB (2010): ALE meta-analysis of action observation and imitation in the human brain. NeuroImage 50:1148–1167.

Caspers S, Eickhoff SB, Rick T, von Kapri A, Kuhlen T, Huang R, Shah NJ, Zilles K (2011): Probabilistic fibre tract analysis of cytoarchitectonically defined human inferior parietal lobule areas reveals similarities to macaques. NeuroImage 58:362–380.

Caspers S, Schleicher A, Bacha-Trams M, Palomero-Gallagher N, Amunts K, Zilles K (2013): Organization of the human inferior parietal lobule based on receptor architectonics. Cereb Cortex 23:615–628.

Catani M, Jones DK, ffytche DH (2005): Perisylvian language networks of the human brain. Ann Neurol 57:8–16.

Chang C, Cunningham JP, Glover GH (2009): Influence of heart rate on the BOLD signal: the cardiac response function. NeuroImage 44:857–869.

Cieslik EC, Zilles K, Caspers S, Roski C, Kellermann TS, Jakobs O, Langner R, Laird AR, Fox PT, Eickhoff SB (2013): Is there "one" DLPFC in cognitive action control? Evidence for heterogeneity from co-activation-based parcellation. Cereb Cortex 23: 2677–2689.

Clos M, Amunts K, Laird AR, Fox PT, Eickhoff SB (2013): Tackling the multifunctional nature of Broca's region meta-analytically: co-activation-based parcellation of area 44. NeuroImage 83:174–188.

Cohen AL, Fair DA, Dosenbach NU, Miezin FM, Dierker D, Van Essen DC, Schlaggar BL, Petersen SE (2008): Defining functional areas in individual human brains using resting functional connectivity MRI. NeuroImage 41:45–57.

Corbetta M, Shulman GL (2002): Control of goal-directed and stimulus-driven attention in the brain. Nat Rev Neurosci 3: 201–215.

Craddock RC, James GA, Holtzheimer PE, 3rd, Hu XP, Mayberg HS (2012): A whole brain fMRI atlas generated via spatially constrained spectral clustering. Hum Brain Mapp 33: 1914–1928.

Craig AD (2002): How do you feel? Interoception: the sense of the physiological condition of the body. Nat Rev Neurosci 3: 655–666.

Craig AD (2003): Interoception: the sense of the physiological condition of the body. Curr Opin Neurobiol 13:500–505.

Critchley HD, Wiens S, Rotshtein P, Ohman A, Dolan RJ (2004): Neural systems supporting interoceptive awareness. Nat Neurosci 7:189–195.

Daw ND, O'Doherty JP, Dayan P, Seymour B, Dolan RJ (2006): Cortical substrates for exploratory decisions in humans. Nature 441:876–879.

Deco G, Ponce-Alvarez A, Mantini D, Romani GL, Hagmann P, Corbetta M (2013): Resting-state functional connectivity emerges from structurally and dynamically shaped slow linear fluctuations. J Neurosci 33:11239–11252.

Deco G, McIntosh AR, Shen K, Hutchison RM, Menon RS, Everling S, Hagmann P, Jirsa VK (2014): Identification of optimal structural connectivity using functional connectivity and neural modeling. J Neurosci 34:7910–7916.

Dice LR (1945): Measures of the amount of ecologic association between species. Ecology 26:297–302.

Eickhoff SB, Grefkes C (2011): Approaches for the integrated analysis of structure, function and connectivity of the human brain. Clin EEG Neurosci 42:107–121.

Eickhoff SB, Stephan KE, Mohlberg H, Grefkes C, Fink GR, Amunts K, Zilles K (2005): A new SPM toolbox for combining probabilistic cytoarchitectonic maps and functional imaging data. NeuroImage 25:1325–1335.

Eickhoff SB, Laird AR, Grefkes C, Wang LE, Zilles K, Fox PT (2009): Coordinate-based activation likelihood estimation meta-analysis of neuroimaging data: a random-effects approach based on empirical estimates of spatial uncertainty. Hum Brain Mapp 30:2907–2926.

Eickhoff SB, Jbabdi S, Caspers S, Laird AR, Fox PT, Zilles K, Behrens TE (2010): Anatomical and functional connectivity of cytoarchitectonic areas within the human parietal operculum. J Neurosci 30:6409–6421.

Eickhoff SB, Bzdok D, Laird AR, Roski C, Caspers S, Zilles K, Fox PT (2011): Co-activation patterns distinguish cortical modules, their connectivity and functional differentiation. NeuroImage 57:938–949.

Eickhoff SB, Bzdok D, Laird AR, Kurth F, Fox PT (2012): Activation likelihood estimation meta-analysis revisited. NeuroImage 59:2349–2361.

Fan J, McCandliss BD, Fossella J, Flombaum JI, Posner MI (2005): The activation of attentional networks. NeuroImage 26: 471–479.

Fan L, Wang J, Zhang Y, Han W, Yu C, Jiang T (2013): Connectivity-based parcellation of the human temporal pole using diffusion tensor imaging. Cereb Cortex 24:3365–3378.

Fan L, Wang J, Zhang Y, Han W, Yu C, Jiang T (2014): Connectivity-based parcellation of the human temporal pole using diffusion tensor imaging. Cereb Cortex 24:3365–3378.

Frey SH, Vinton D, Norlund R, Grafton ST (2005): Cortical topography of human anterior intraparietal cortex active during visually guided grasping. Brain Res Cognit Brain Res 23: 397–405.

Gallagher HL, Happe F, Brunswick N, Fletcher PC, Frith U, Frith CD (2000): Reading the mind in cartoons and stories: an fMRI study of 'theory of mind' in verbal and nonverbal tasks. Neuropsychologia 38:11–21.

Gorno-Tempini ML, Dronkers NF, Rankin KP, Ogar JM, Phengrasamy L, Rosen HJ, Johnson JK, Weiner MW, Miller BL (2004): Cognition and anatomy in three variants of primary progressive aphasia. Ann Neurol 55:335–346.

Gotts SJ, Jo HJ, Wallace GL, Saad ZS, Cox RW, Martin A (2013a): Two distinct forms of functional lateralization in the human brain. Proc Natl Acad Sci U S A 110:E3435–E3444.

Gotts SJ, Saad ZS, Jo HJ, Wallace GL, Cox RW, Martin A (2013b): The perils of global signal regression for group comparisons: a

case study of Autism Spectrum Disorders. Front Human Neurosci 7:356.

Graves WW, Desai R, Humphries C, Seidenberg MS, Binder JR (2010): Neural systems for reading aloud: a multiparametric approach. Cereb Cortex 20:1799–1815.

Greicius MD, Supekar K, Menon V, Dougherty RF (2009): Resting-state functional connectivity reflects structural connectivity in the default mode network. Cereb Cortex 19:72–78.

Hagmann P, Cammoun L, Gigandet X, Meuli R, Honey CJ, Wedeen VJ, Sporns O (2008): Mapping the structural core of human cerebral cortex. PLoS Biol 6:e159.

Hickok G, Poeppel D (2000): Towards a functional neuroanatomy of speech perception. Trends Cogn Sci 4:131–138.

Honey CJ, Sporns O, Cammoun L, Gigandet X, Thiran JP, Meuli R, Hagmann P (2009): Predicting human resting-state functional connectivity from structural connectivity. Proc Natl Acad Sci U S A 106:2035–2040.

Johansen-Berg H, Behrens TE, Robson MD, Drobnjak I, Rushworth MF, Brady JM, Smith SM, Higham DJ, Matthews PM (2004): Changes in connectivity profiles define functionally distinct regions in human medial frontal cortex. Proc Natl Acad Sci U S A 101:13335–13340.

Kelly C, Toro R, Di Martino A, Cox CL, Bellec P, Castellanos FX, Milham MP (2012): A convergent functional architecture of the insula emerges across imaging modalities. NeuroImage 61:1129–1142.

Kim JH, Lee JM, Jo HJ, Kim SH, Lee JH, Kim ST, Seo SW, Cox RW, Na DL, Kim SI, Saad ZS (2010): Defining functional SMA and pre-SMA subregions in human MFC using resting state fMRI: functional connectivity-based parcellation method. NeuroImage 49:2375–2386.

Koch MA, Norris DG, Hund-Georgiadis M (2002): An investigation of functional and anatomical connectivity using magnetic resonance imaging. NeuroImage 16:241–250.

Laird AR, Eickhoff SB, Rottschy C, Bzdok D, Ray KL, Fox PT (2013): Networks of task co-activations. NeuroImage 80:505–514.

Li W, Qin W, Liu H, Fan L, Wang J, Jiang T, Yu C (2013): Subregions of the human superior frontal gyrus and their connections. NeuroImage 78:46–58.

Liu H, Qin W, Li W, Fan L, Wang J, Jiang T, Yu C (2013): Connectivity-based parcellation of the human frontal pole with diffusion tensor imaging. J Neurosci 33:6782–6790.

Makris N, Pandya DN (2009): The extreme capsule in humans and rethinking of the language circuitry. Brain Struct Funct 213:343–358.

Makris N, Kennedy DN, McInerney S, Sorensen AG, Wang R, Caviness VS Jr., Pandya DN (2005): Segmentation of subcomponents within the superior longitudinal fascicle in humans: a quantitative, in vivo, DT-MRI study. Cereb Cortex 15:854–869.

Mar RA (2011): The neural bases of social cognition and story comprehension. Annu Rev Psychol 62:103–134.

Mars RB, Jbabdi S, Sallet J, O'Reilly JX, Croxson PL, Olivier E, Noonan MP, Bergmann C, Mitchell AS, Baxter MG, Behrens TE, Johansen-Berg H, Tomassini V, Miller KL, Rushworth MF (2011): Diffusion-weighted imaging tractography-based parcellation of the human parietal cortex and comparison with human and macaque resting-state functional connectivity. J Neurosci 31:4087–4100.

Mars RB, Sallet J, Schuffelgen U, Jbabdi S, Toni I, Rushworth MF (2012): Connectivity-based subdivisions of the human right "temporoparietal junction area": evidence for different areas participating in different cortical networks. Cereb Cortex 22:1894–1903.

Mevorach C, Humphreys GW, Shalev L (2009): Reflexive and preparatory selection and suppression of salient information in the right and left posterior parietal cortex. J Cognit Neurosci 21:1204–1214.

Mort DJ, Perry RJ, Mannan SK, Hodgson TL, Anderson E, Quest R, McRobbie D, McBride A, Husain M, Kennard C (2003): Differential cortical activation during voluntary and reflexive saccades in man. NeuroImage 18:231–246.

Nebel MB, Joel SE, Muschelli J, Barber AD, Caffo BS, Pekar JJ, Mostofsky SH (2012): Disruption of functional organization within the primary motor cortex in children with autism. Hum Brain Mapp 35:567–580.

Nebel MB, Joel SE, Muschelli J, Barber AD, Caffo BS, Pekar JJ, Mostofsky SH (2014): Disruption of functional organization within the primary motor cortex in children with autism. Hum Brain Mapp 35:567–580.

Nee DE, Wager TD, Jonides J (2007): Interference resolution: insights from a meta-analysis of neuroimaging tasks. Cognit Affect Behav Neurosci 7:1–17.

Neubert FX, Mars RB, Thomas AG, Sallet J, Rushworth MF (2014): Comparison of human ventral frontal cortex areas for cognitive control and language with areas in monkey frontal cortex. Neuron 81:700–713.

Power JD, Cohen AL, Nelson SM, Wig GS, Barnes KA, Church JA, Vogel AC, Laumann TO, Miezin FM, Schlaggar BL, Petersen SE (2011): Functional network organization of the human brain. Neuron 72:665–678.

Raine A, Yang Y (2006): Neural foundations to moral reasoning and antisocial behavior. Social Cognit Affect Neurosci 1:203–213.

Rizzolatti G (2005): The mirror neuron system and its function in humans. Anat Embryol 210:419–421.

Robinson JL, Laird AR, Glahn DC, Lovallo WR, Fox PT (2010): Meta-analytic connectivity modeling: delineating the functional connectivity of the human amygdala. Hum Brain Mapp 31:173–184.

Rottschy C, Caspers S, Roski C, Reetz K, Dogan I, Schulz JB, Zilles K, Laird AR, Fox PT, Eickhoff SB (2013): Differentiated parietal connectivity of frontal regions for "what" and "where" memory. Brain Struct Funct 218:1551–1567.

Ruschel M, Knosche TR, Friederici AD, Turner R, Geyer S, Anwander A (2014): Connectivity architecture and subdivision of the human inferior parietal cortex revealed by diffusion MRI. Cereb Cortex 24:2436–2448.

Saad ZS, Reynolds RC, Jo HJ, Gotts SJ, Chen G, Martin A, Cox RW (2013): Correcting brain-wide correlation differences in resting-state FMRI. Brain Connect 3:339–352.

Sallet J, Mars RB, Noonan MP, Neubert FX, Jbabdi S, O'Reilly JX, Filippini N, Thomas AG, Rushworth MF (2013): The organization of dorsal frontal cortex in humans and macaques. J Neurosci 33:12255–12274.

Skudlarski P, Jagannathan K, Calhoun VD, Hampson M, Skudlarska BA, Pearlson G (2008): Measuring brain connectivity: diffusion tensor imaging validates resting state temporal correlations. NeuroImage 43:554–561.

Smith BD, Meyers M, Kline R, Bozman A (1987): Hemispheric asymmetry and emotion: lateralized parietal processing of affect and cognition. Biol Psychol 25:247–260.

Smith SM, Fox PT, Miller KL, Glahn DC, Fox PM, Mackay CE, Filippini N, Watkins KE, Toro R, Laird AR, Beckmann CF (2009): Correspondence of the brain's functional architecture during activation and rest. Proc Natl Acad Sci U S A 106:13040–13045.

Spreng RN, Mar RA, Kim AS (2009): The common neural basis of autobiographical memory, prospection, navigation, theory of mind, and the default mode: a quantitative meta-analysis. J Cognit Neurosci 21:489–510.

Thiebaut de Schotten M, Dell'Acqua F, Forkel SJ, Simmons A, Vergani F, Murphy DG, Catani M (2011): A lateralized brain network for visuospatial attention. Nat Neurosci 14: 1245–1246.

Thiel CM, Zilles K, Fink GR (2004): Cerebral correlates of alerting, orienting and reorienting of visuospatial attention: an event-related fMRI study. NeuroImage 21:318–328.

Tomassini V, Jbabdi S, Klein JC, Behrens TE, Pozzilli C, Matthews PM, Rushworth MF, Johansen-Berg H (2007): Diffusion-weighted imaging tractography-based parcellation of the human lateral premotor cortex identifies dorsal and ventral subregions with anatomical and functional specializations. J Neurosci 27:10259–10269.

Uddin LQ, Supekar K, Amin H, Rykhlevskaia E, Nguyen DA, Greicius MD, Menon V (2010): Dissociable connectivity within human angular gyrus and intraparietal sulcus: evidence from functional and structural connectivity. Cereb Cortex 20:2636–2646.

Van den Heuvel MP, Mandl RC, Kahn RS, Hulshoff Pol HE (2009): Functionally linked resting-state networks reflect the underlying structural connectivity architecture of the human brain. Hum Brain Mapp 30:3127–3141.

Vesia M, Monteon JA, Sergio LE, Crawford JD (2006): Hemispheric asymmetry in memory-guided pointing during single-pulse transcranial magnetic stimulation of human parietal cortex. J Neurophysiol 96:3016–3027.

Vossel S, Thiel CM, Fink GR (2006): Cue validity modulates the neural correlates of covert endogenous orienting of attention in parietal and frontal cortex. NeuroImage 32:1257–1264.

Wager TD, Sylvester CY, Lacey SC, Nee DE, Franklin M, Jonides J (2005): Common and unique components of response inhibition revealed by fMRI. NeuroImage 27:323–340.

Wang J, Fan L, Zhang Y, Liu Y, Jiang D, Zhang Y, Yu C, Jiang T (2012): Tractography-based parcellation of the human left inferior parietal lobule. NeuroImage 63:641–652.

Wang J, Fan L, Wang Y, Xu W, Jiang T, Fox PT, Eickhoff SB, Yu C, Jiang T (2015a): Determination of the posterior boundary of Wernicke's area based on multimodal connectivity profiles. Hum Brain Mapp 36:1908–1924.

Wang J, Yang Y, Fan L, Xu J, Li C, Liu Y, Fox PT, Eickhoff SB, Yu C, Jiang T (2015b): Convergent functional architecture of the superior parietal lobule unraveled with multimodal neuroimaging approaches. Hum Brain Mapp 36:238–257.

Wu Y, Wang J, Zhang Y, Zheng D, Zhang J, Rong M, Wu H, Wang Y, Zhou K, Jiang T (2016): The neuroanatomical basis for posterior superior parietal lobule control lateralization of visuospatial attention. Front Neuroanat 10:32.

Zhang D, Snyder AZ, Shimony JS, Fox MD, Raichle ME (2010): Noninvasive functional and structural connectivity mapping of the human thalamocortical system. Cereb Cortex 20: 1187–1194.

Zhang Y, Fan L, Zhang Y, Wang J, Zhu M, Zhang Y, Yu C, Jiang T (2014): Connectivity-based parcellation of the human posteromedial cortex. Cereb Cortex 24:719–727.